International Conference on Mathematics, Computational Methods & Reactor Physics (M&C 2009)
Saratoga Springs, New York, May 3-7, 2009, on CD-ROM, American Nuclear Society, LaGrange Park, IL (2009)

ANALYSIS OF DISTANCES BETWEEN INCLUSIONS IN FINITE ONE-DIMENSIONAL BINARY STOCHASTIC MATERIALS

David P. Griesheimer
Bettis Atomic Power Laboratory
P.O. Box 79
grieshei@bettis.gov

David L. Millman
Department of Computer Science
The University of North Carolina at Chapel Hill
Chapel Hill, NC 27599
dave@cs.unc.edu

ABSTRACT

In this paper we develop a statistical distribution for the number of inclusions present in a one-dimensional binary stochastic material of a finite length. From this distribution, an analytic solution for the expected number of inclusions present in a given problem is derived. For cases where the analytical solution for the expected number of inclusions is prohibitively expensive to compute, a simple, empirically-derived, approximation for the expected value is presented. A series of numerical experiments are used to bound the error of this approximation over the domain of interest. Finally, the above approximations are used to develop a methodology for determining the distribution of distances between adjacent inclusions in the material, subject to known problem conditions including: the total length of the problem, the length of each inclusion, and the expected volume fraction of inclusions in the problem. The new method is shown to be equivalent to the use of the infinite medium nearest neighbor distribution with an effective volume fraction to account for the finite nature of the material. Numerical results are presented for a wide range of problem parameters, in order to demonstrate the accuracy of this method and identify conditions where the method breaks down. In general, the technique is observed to produce excellent results (absolute error less than 1×10^{-6}) for problems with inclusion volume fractions less than 0.8 and a ratio of problem length to inclusion length greater than 25. For problems that do not fall into this category, the accuracy of the method is shown to be dependent on the particular combination of these parameters. A brief discussion of the relevance of this method for Monte Carlo chord length sampling algorithms is also provided.

Key Words: Stochastic Mixture, Monte Carlo, Chord Length Sampling, Stochastic Transport

1. INTRODUCTION

Over the past 20 years, a significant amount of research has been devoted to developing methods for solving the linear transport equation in random heterogeneous mixtures of two or more distinct materials [1-12]. The resulting methods have been successfully applied to a wide variety of problems, including the modeling of radiation transport through heterogeneous materials such as concrete, water droplets in the atmosphere, gas/dust in interstellar space, two-phase gas-liquid mixtures, biological tissue, TRISO fuel particles (commonly found in High Temperature Gas

Reactor (HTGR) fuel), and certain thermal neutron poison materials used for criticality safety applications (marketed under the trade name BORAL®) [2-10]. In each of these cases, the transport medium can be modeled as a stochastic mixture of homogeneous inclusions, which are randomly distributed within a uniform background material. Solving the linear transport equation for this type of mixture, referred to as a *stochastic material*, presents a unique set of challenges. The random distribution of inclusions within the mixture means that the properties (e.g. cross sections) for a stochastic material have a strong spatial dependence. Furthermore, this spatial dependence is unique for every particular realization of the material, implying that the transport solution itself must be dependent on the detailed arrangement of inclusions within the material. Unfortunately, for most cases of interest, it is impractical to consider explicitly modeling every inclusion in the material. Even if the inclusions were stationary with known locations, which they typically are not, the actual transport calculation would be prohibitively expensive for large numbers of inclusions. Instead, it is more practical to search for an "average" transport solution, which is reasonably accurate over a wide range of material realizations. References 3 and 4 provide a thorough review of the previous methods development work in this area.

Recently, Monte Carlo methods have gained widespread use for analyzing stochastic media transport problems. Unfortunately, brute force approaches for calculating the ensemble average solutions with Monte Carlo methods are severely limited by the availability of computer resources. As noted earlier, the explicit representation of individual inclusions within a stochastic material is impractical for all but the smallest problems. To overcome these problems, Zimmerman and Adams [2] proposed a new technique for Monte Carlo transport calculations, which does not require inclusions to be explicitly represented. In their chord-length sampling (CLS) method, the distances between and within inclusions in a stochastic material are randomly sampled from appropriate statistical distributions during the particle transport process.

By sampling the distances between material interfaces (background/inclusion or inclusion/ background) on the fly, the CLS method is able to track particles through stochastic materials very efficiently. Furthermore, by only considering the distances between material interfaces that occur along the current particle flight path, the CLS method effectively reduces multi-dimensional particle tracking in a stochastic material to a series of simpler one-dimensional ray tracing calculations, which are easier to compute and analyze theoretically. In numerical experiments, variants of the CLS method have repeatedly shown excellent performance and good agreement with benchmark results [2-9, 11].

However, while the CLS method has shown promising results for many benchmark calculations, there are still a number of open questions regarding its use in more realistic problems. In particular, the results of the CLS are known to be strongly dependent on the statistical distributions used to describe the stochastic material. While chord length distributions within slab (1-D), disk (2-D), and spherically (3-D) shaped inclusions are well known [3,12], the distribution of distances between adjacent inclusions has not been well characterized, until recently. In ideal cases, it is known that the distribution of distances between adjacent inclusions should be exponentially distributed with a constant rate parameter [12], which we will denote λ. Past CLS studies have relied on empirical fitting calculations to determine λ for a particular problem of interest [3-7]. These empirically produced values have typically yielded good

agreement with numerical experiments. However, requiring an empirically fit rate parameter to be calculated for each unique problem was viewed as a limitation of the original CLS models. These methods would be much more convenient and applicable if the rate parameter could be calculated, or at least estimated, on the fly, thus eliminating the need for auxiliary fitting calculations. To this end, recent work by Ji and Martin [9, 11] has considered the distribution of distances between fuel microspheres in pebble and compact-type VTHR fuel elements. For three dimensional problems, their result matches the theoretical distribution of distributions for uniformly distributed spheres in an infinite medium [11]. However, subsequent analysis has shown that this limiting distribution may not be an accurate approximation near the edges of stochastic materials with finite extent. This boundary effect is due to the fact that the volume fraction of inclusions is lower near the edge of a region than in the center, due to limitations on allowable particle locations near the boundary [11]. Previous work by Murata *et. al.* [6,7]and Ji and Martin [11] has shown that it is possible to apply correction factors to the infinite medium results in order to account for these boundary effects. In these studies, the boundary correction was applied through the use of a modified inclusion volume fraction, which takes into account the size and geometry of the stochastic material region. In addition, Ji and Martin [11] have developed a methodology for calculating a problem specific correction factor through the use of simple fitting calculations.

In this paper we seek to develop a better understanding of the boundary effect by analyzing the distribution of distances between adjacent inclusions in a 1-D binary stochastic media problem with finite length. We begin by developing a statistical distribution for the number of fixed-length inclusions present in a one-dimensional slab of total length L. From this distribution, an analytic solution for the expected number of inclusions present in a given problem is derived. For cases where the analytical solution for the expected number of inclusions is prohibitively expensive to compute, a simple, empirically-derived, approximation for the expected value is presented. A series of numerical experiments are used to bound the error of this approximation over the domain of interest. Finally, the above approximations are used to develop a methodology for determining the rate parameter that characterizes the distribution of distances between adjacent inclusions in the material, subject to known problem conditions including: the total length of the problem, the length of each inclusion, and the expected total volume fraction of inclusions in the problem. Numerical results are presented for a wide range of problem parameters, in order to demonstrate the accuracy of this method and identify conditions where the method breaks down.

The results from this paper demonstrate that the distribution of distances between adjacent inclusions in a 1-D binary stochastic mixture can be well modeled by an exponential distribution for realistic cases. The proposed methodology for estimating the unknown rate parameter λ is shown to produce excellent results (absolute error less than 1×10^{-6}) for problems with inclusion volume fractions less than 0.8 and a ratio of problem length to inclusion length greater than 25. For problems that do not fall into this category, the accuracy of the method is shown to be dependent on the particular combination of these parameters. While the results provided in this paper are specifically for 1-D problems, the authors believe that the understanding developed on this academic problem provides significant insight into higher-dimensional problems.

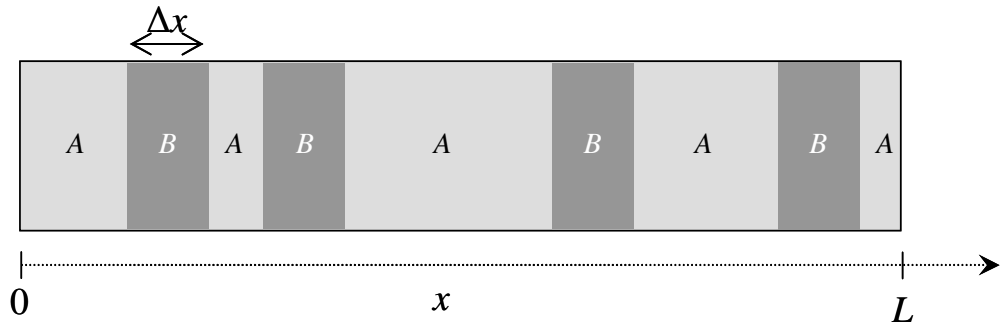

Figure 1. Illustration of a one-dimensional binary stochastic material with total length *L*, and inclusion length Δ*x*.

2. DERIVATION OF THE EXPECTED NUMBER OF INCLUSIONS

2.1. Assumptions

For this analysis we will consider a one-dimensional slab of length *L*, which contains a number of inclusions of fixed length Δ*x* distributed randomly throughout. The background material of the slab is identified as material *A*, and the material in the inclusions is identified as material *B*. Both the number and spatial location of the inclusions is assumed to be random, subject to the conditions that no inclusion may extend beyond the boundaries of the slab and no two inclusions may overlap with one another. An illustration of an example slab of this type is shown in Figure 1. In this section we seek to derive statistical distributions that describe both the number of inclusions in a slab, and also the distribution of distances that separate two adjacent inclusions.

We begin the derivations by assuming that the distance between any two adjacent inclusions can be well-described by an exponential distribution of the form

$$p_{\exp}(x;\lambda) = \begin{cases} \lambda\, e^{-\lambda x}, & x \geq 0 \\ 0, & x < 0 \end{cases}, \tag{1}$$

where x is the distance between inclusions and λ is a rate parameter, which determines the probability of encountering an inclusion per distance traveled. As noted earlier, this assumption is known to be exact for ideal (infinite medium) cases [12], and has also been shown to produce accurate results in certain non-ideal (typically thick media) problems [4,9,11]. In this paper we will consider the validity of this assumed distribution for different combinations of slab length (L) and inclusion thickness (Δx). We proceed by deriving a probability density function for the number of inclusions in a slab of total length L, based on the assumed distribution of distances (chords) between adjacent inclusions, as given in Eq. (1).

2.2. Single Inclusion Case

Before deriving the distribution for a slab with multiple inclusions, let us first consider a simpler two-region problem that contains a random-length segment of material *A* followed by a single

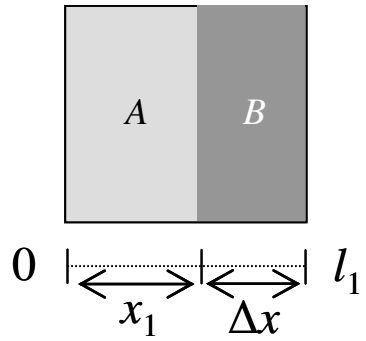

Figure 2. Illustration of a one-dimensional binary stochastic material containing exactly one inclusion. In this case the length of the slab l_1 is a random variable.

inclusion of material *B*, as shown in Figure 2. In this case, the length of the material *A* segment, x_1, is a realization of the random variable *X*, which is governed by the probability distribution $p_{exp}(x; \lambda)$. The total length of the simple two-region problem is equal to

$$l_1 = x_1 + \Delta x\,, \tag{2}$$

The probability of finding no inclusions in a fixed length *L* is equal to the probability that $l_1 > L$, or, correspondingly, the probability that $x_1 > L - \Delta x$. From the probability distribution given in Eq. (1) we can show

$$p\left(x > L - \Delta x\right) = \int_{L-\Delta x}^{\infty} \lambda\, e^{-\lambda x} dx\,. \tag{3}$$

Evaluating the integral in Eq. (3) yields an expression for the probability

$$p\left(N = 0\right) = e^{-\lambda\left(L-\Delta x\right)}\,, \tag{4}$$

where *N* is the number of inclusions in the slab. We note that Eq. (4) agrees with the $N = 0$ result previously derived by Donovan and Dannon [4]. In cases where the total length of the slab is so narrow that more than one inclusion cannot fit ($L < 2\,\Delta x$), we can immediately calculate the probability of finding an inclusion in the slab by the relationship, $p(N = 1) = 1 - p(N = 0)$. However, for cases where $L < 2\,\Delta x$ we must consider the possibility of multiple inclusions occurring within the slab.

2.3. Multiple Inclusion Case

For slabs containing more than one inclusion, we immediately recognize that any slab containing multiple inclusions may be broken up into a series of two-region segments of the form described in the previous section. Under this partitioning, the length of the material *A* region in each segment is an independent realization from the random variable *X*. Therefore, the total length of *n* segments, L_n, can be calculated by summing Eq. (2) over *n* independent realizations from *X*,

$$L_n = \sum_{i=1}^{n} x_i + \Delta x \,. \tag{5}$$

Since the length of the inclusions is a constant value, we may factor this term out of the summation and rewrite Eq. (5) as

$$L_n = n\Delta x + \sum_{i=1}^{n} x_i \,. \tag{6}$$

Because the realizations of X are guaranteed to be positive, L_n must be a monotonically increasing function of n. Therefore, for any given sequence of realizations $\{x_1, x_2, x_3, \ldots\}$ there exists a value n' such that $L_{n'+j} > L$ for all $j \geq 1$. Thus n' gives the number of inclusions that occur in a slab of length L for a given sequence of realizations $\{x_1, x_2, x_3, \ldots\}$. Additional inclusions are not possible because they will not fit within the given slab length, L.

Using this information, we wish to determine the probability that a given number of inclusions, N, will occur within a slab of length L. We begin by determining the probability that $L_n > L$, implying that n inclusions will not fit in a slab of length L. From Eq. (6) we write

$$p\left(L_n > L\right) = p\left(n\Delta x + \sum_{i=1}^{n} x_i > L\right). \tag{7}$$

From the left hand side of Eq. (7) we note that when $L_n > L$, the actual number of inclusions in the slab, N, must be less than or equal to $n-1$,

$$p\left(N \leq n-1\right) = p\left(\sum_{i=1}^{n} x_i > L - n\Delta x\right). \tag{8}$$

The right hand side of Eq. (8) is the probability that the sum of n independent identically distributed random variables will be greater than a constant value. Writing this sum as a new random variable Y_n, we have

$$y_n = \sum_{i=1}^{n} x_i \,. \tag{9}$$

In the case where the x_i realizations are all taken from an identical exponential distribution with rate parameter λ, it can be shown that the y_n values are Erlang distributed with probability

$$p_{\mathrm{Er}}\left(y; n, \lambda\right) = \frac{\lambda^n y^{n-1} e^{-\lambda y}}{\left(n-1\right)!}\,, \tag{10}$$

and cumulative probability,

$$P_{\mathrm{Er}}\left(y;n,\lambda\right)=\frac{\gamma\left(n,\lambda y\right)}{\left(n-1\right)!}, \tag{11}$$

where $\gamma(n,\lambda y)$ is the lower incomplete gamma function, which is defined by

$$\gamma\left(n,\lambda y\right)=\int_0^{\lambda y} t^{n-1}e^{-t}dt\,. \tag{12}$$

Substituting Eq. (9) and (10) into Eq. (8) yields

$$p\left(N\le n-1\right)=p\left(y_n>L-n\Delta x\right)=\int_{L-n\Delta x}^{\infty} p_{Er}\left(y;n,\lambda\right)dy\,. \tag{13}$$

The right hand side of Eq. (13) can be rewritten in terms of the cumulative probability distribution, P_{Er}, by

$$p\left(N\le n-1\right)=\int_0^{\infty} p_{\mathrm{Er}}\left(y;n,\lambda\right)dy-\int_0^{L-n\Delta x} p_{\mathrm{Er}}\left(y;n,\lambda\right)dy$$

$$p\left(N\le n-1\right)=1-P_{\mathrm{Er}}\left(y;n,\lambda\left(L-n\Delta x\right)\right). \tag{14}$$

Substituting Eq. (11) in to Eq. (14) gives the cumulative distribution function

$$P\left(n-1\right)=p\left(N\le n-1\right)=1-\frac{\gamma\left(n,\lambda\left(L-n\Delta x\right)\right)}{\left(n-1\right)!}. \tag{15}$$

Now that we have determined the probability that there are $n-1$ or fewer inclusions we can determine the probability that there are exactly n inclusions by noting that

$$p\left(N=n\right)=p\left(N\le n\right)-p\left(N\le n-1\right). \tag{16}$$

Substituting Eq. (15) for $N\le n$ and $N\le n-1$ into Eq. (16) gives the final result

$$p\left(N\right)=\frac{\gamma\left(N,\lambda\left(L-N\Delta x\right)\right)}{\left(N-1\right)!}-\frac{\gamma\left(N+1,\lambda\left(L-(N+1)\Delta x\right)\right)}{N!}. \tag{17}$$

2.4. Generalized Probability Distribution Function

By examination we see that the probability distribution function given in Eq. (17) is not well defined for cases where $N\le 0$ (due to $N-1$ factorial in first term) or $N>L/\Delta x\ -1$ (due to the argument of the gamma function in the second term). The expression for $p(N=0)$ was derived in the previous section (Eq. (4)) and shown to be

$$p\left(N=0\right)=e^{-\lambda\left(L-\Delta x\right)}, \tag{4}$$

which can be rewritten in terms of the incomplete gamma function, Eq. (12), to yield

$$p\left(N=0\right)=1-\gamma\left(1,\lambda\left(L-\Delta x\right)\right). \tag{18}$$

Understanding the behavior of $p(N)$ for $N > L/\Delta x - 1$ requires a little more effort. Returning to the cumulative distribution function defined in Eq. (15) we can show that, for cases where the slab length is an integer multiple of the inclusion thickness ($L/\Delta x \in \mathbb{Z}^+$, where $\mathbb{Z}^+$ is the set of positive integers),

$$p\left(N\le {L}/{\Delta x}-1\right)=1-\frac{\gamma\left({L}/{\Delta x},\lambda\left(L-{L}/{\Delta x}\,\Delta x\right)\right)}{\left({L}/{\Delta x}\right)!}$$

$$p\left(N\le {L}/{\Delta x}-1\right)=1-\frac{\gamma\left({L}/{\Delta x},0\right)}{\left({L}/{\Delta x}\right)!}=1, \tag{19}$$

by the definition of the lower incomplete gamma function, given in Eq. (12). The result shown in Eq. (19) demonstrates that, for cases where the slab length, L, is an integer multiple of the inclusion length, Δx, the probability of observing $N > L/\Delta x - 1$ inclusions is zero.

For cases where the slab length is not an integer multiple of the inclusion length, the corresponding analysis becomes more complicated. Because the probability distribution for the number of inclusions (Eq. (15)) is a discrete valued function, we cannot calculate the probability that N is less than or equal to a non-integer value. However, we can calculate the probability that N is less than or equal to the nearest integer below $L/\Delta x - 1$. For this case we can show that

$$p\left(N\le \left\lfloor {L}/{\Delta x}\right\rfloor -1\right)=1-\frac{\gamma\left(\left\lfloor {L}/{\Delta x}\right\rfloor,\lambda\left(L-\left\lfloor {L}/{\Delta x}\right\rfloor \Delta x\right)\right)}{\left(\left\lfloor {L}/{\Delta x}\right\rfloor\right)!}$$

$$p\left(N\le \left\lfloor {L}/{\Delta x}\right\rfloor -1\right)=1-\frac{\gamma\left(\left\lfloor {L}/{\Delta x}\right\rfloor,\lambda\,\Delta x\,f\right)}{\left(\left\lfloor {L}/{\Delta x}\right\rfloor\right)!}<1, \tag{20}$$

where $\lfloor L/\Delta x \rfloor$ denotes the closest integer below the real value $L/\Delta x$, and $f=\left(L/\Delta x-\lfloor L/\Delta x\rfloor\right)$ is the fractional part of $\lfloor L/\Delta x \rfloor$, which is guaranteed to fall between 0 and 1. The result shown in Eq. (20) demonstrates that there is a non-zero probability of observing $N>\lfloor L/\Delta x\rfloor -1$ inclusions in the slab. In addition, we can also recognize that it is physically impossible to allow $N\ge\lfloor L/\Delta x\rfloor +1$ inclusions in the slab, as the total length of the $\lfloor L/\Delta x\rfloor +1$ inclusions is $\Delta x\left(\lfloor L/\Delta x\rfloor +1\right)=L+\Delta x\left(1-f\right)$, which is greater than the length of the slab, L. Therefore, we

conclude that the probability of observing $N > \lfloor L/\Delta x \rfloor$ inclusions must be zero. From the above discussion, it is clear that

$$p\left(N > \left\lfloor {}^{L}\!/_{\Delta x} \right\rfloor\right) = 0 \tag{21}$$

for all cases, and

$$p\left(N > \left\lfloor {}^{L}\!/_{\Delta x} \right\rfloor - 1\right) = 0 \tag{22}$$

when $L/\Delta x \in \mathbb{Z}$.

Using the results given in Eqs. (17), (18), (21) and (22), we can now write the probability distribution for the number of inclusions in a slab of total length L as

$$p(N) = \begin{cases} 1 - \gamma\left(1, \lambda\left(L - \Delta x\right)\right) & N = 0 \\ \dfrac{\gamma\left(N, \lambda\left(L - N\Delta x\right)\right)}{(N-1)!} - \dfrac{\gamma\left(N+1, \lambda\left(L - (N+1)\Delta x\right)\right)}{N!} & \begin{cases} 0 < N \le \dfrac{L}{\Delta x} - 1, & \dfrac{L}{\Delta x} \in \mathbb{Z} \\ 0 < N \le \left\lfloor \dfrac{L}{\Delta x} \right\rfloor, & \dfrac{L}{\Delta x} \notin \mathbb{Z} \end{cases} \\ 0 & \text{Other} \end{cases}. \tag{23}$$

Before continuing, we wish to take a moment to remind the reader that preceding derivations and resulting probability distribution function are exact <u>if</u> the distances between adjacent inclusions are exponentially distributed with constant rate parameter λ.

2.5. Limiting Behaviors of *p*(*N*)

The probability distribution function given in Eq. (23) is a complicated, non-intuitive, function of both slab length (L) and inclusion width (Δx). In order to gain understanding about the function $p(N)$ it is useful to consider the limiting behavior of the function for both large and small inclusion widths.

In the first case, we will consider the behavior of $p(N)$ as the inclusion width Δx becomes small. Because $p(N)$ has a piecewise definition, we will proceed by treating the functions for $N = 0$ and $N > 0$ separately. From Eqs. (23), (18), and (4) we immediately see that, for $N = 0$,

$$\lim_{\Delta x \to 0} p(N) = e^{-\lambda L} \quad (\text{for } N = 0). \tag{24}$$

In the case where N > 0, we begin by taking the limit of Eq. (23) as $\Delta x \to 0$,

$$\lim_{\Delta x\to 0} p(N) = \frac{\gamma(N,\lambda L)}{(N-1)!} - \frac{\gamma(N+1,\lambda L)}{N!}. \tag{25}$$

To proceed, we make use of a recurrence relationship for the incomplete gamma function [13], which allows $\gamma(N+1, \lambda L)$ to be written in terms of $\gamma(N, \lambda L)$,

$$\gamma(N+1,\lambda L) = N\gamma(N,\lambda L) - (\lambda L)^N e^{-\lambda L}. \tag{26}$$

Substituting Eq. (26) into (25) and simplifying yields,

$$\lim_{\Delta x\to 0} p(N) = \frac{\gamma(N,\lambda L)}{(N-1)!} - \frac{N\gamma(N,\lambda L) - (\lambda L)^N e^{-\lambda L}}{N!},$$

$$\lim_{\Delta x\to 0} p(N) = \frac{(\lambda L)^N e^{-\lambda L}}{N!} \quad (\text{for } N>0). \tag{27}$$

Combining Eqs. (24) and (27) gives the final result,

$$\lim_{\Delta x\to 0} p(N) = \frac{(\lambda L)^N e^{-\lambda L}}{N!} = p_{\text{pois}}(N;\lambda L), \tag{28}$$

where $p_{\text{pois}}(N; \lambda L)$ is the Poisson distribution. Thus we see that as the inclusion width approaches zero, the number of inclusions in the slab approaches a Poisson distribution.

For the second limiting case, we will consider the behavior of $p(N)$ as the inclusion width Δx becomes large ($\Delta x \to L$). For values of $\Delta x > L/2$, Eq. (23) simplifies to the single inclusion distribution function discussed in section 2.2,

$$p(N) = \begin{cases} 1-\gamma(1,\lambda(L-\Delta x)) & N=0 \\ \gamma(1,\lambda(L-\Delta x)) & N=1 \end{cases}. \tag{29}$$

The expected value of the distribution given in Eq. (29) can be easily calculated,

$$R \equiv E\left[p(N)\right] = \gamma(1,\lambda(L-\Delta x)), \tag{30}$$

where R is defined as the probability of finding an inclusion in the slab. Substituting Eq. (30) into Eq. (29) allows the single inclusion probability distribution function to be written in terms of R,

$$p(N) = \begin{cases} 1-R & N=0 \\ R & N=1 \end{cases}, \tag{31}$$

which is the Bernoulli distribution with the variable R as the probability of success. Thus we see that, in cases where the inclusion width is greater than half the total slab length, the observation of an inclusion in the slab reduces to a Bernoulli experiment; for each trial there is some fixed probability of finding an inclusion in the slab.

2.6. Expected Number of Inclusions in a Slab

Now that we have developed an analytical formula for the probability of finding exactly N inclusions in a slab of total length L, we can calculate the expected number of inclusions in the slab,

$$\langle N \rangle = \sum_{n=0}^{\infty} n\, p(n). \tag{32}$$

Applying the condition that $p(n) = 0$ for $n > \lfloor L/\Delta x \rfloor$, Eq. (21), allows us to rewrite Eq. (32) as a finite sum

$$\langle N \rangle = \sum_{n=0}^{\lfloor L/\Delta x \rfloor} n\, p(n). \tag{33}$$

Equation (33) is in a convenient form for a summation by parts transformation, which allows a finite sum of two factors f and g to be rewritten as

$$\sum_{n=0}^{k} f_n\, g_n = f_k \sum_{j=0}^{k} g_j - \sum_{n=0}^{k-1} (f_{n+1} - f_n) \sum_{j=0}^{n} g_j\ . \tag{34}$$

Applying Eq. (34) with $f_n = n$ and $g_n = p(n)$ allows Eq. (33) to be rewritten as

$$\sum_{n=0}^{\lfloor L/\Delta x \rfloor} n\, p(n) = \lfloor L/\Delta x \rfloor \sum_{j=0}^{\lfloor L/\Delta x \rfloor} p(j) - \sum_{n=0}^{\lfloor L/\Delta x \rfloor - 1} (n+1-n) \sum_{j=0}^{n} p(j). \tag{35}$$

By noting that the first summation over j is equal to 1, by Eq. (21), and the second summation over j is the cumulative distribution function $P(n)$, we can rewrite Eq. (35) as

$$\sum_{n=0}^{\lfloor L/\Delta x \rfloor} n\, p(n) = \lfloor L/\Delta x \rfloor - \sum_{n=0}^{\lfloor L/\Delta x \rfloor - 1} P(n)\ . \tag{36}$$

Factoring the first term on the right hand side of Eq. (36) into the summation yields

$$\sum_{n=0}^{\lfloor L/\Delta x \rfloor} n\, p(n) = \sum_{n=0}^{\lfloor L/\Delta x \rfloor - 1} 1 - P(n)\ . \tag{37}$$

Substituting the definition for the cumulative distribution function, Eq. (15), into Eq. (37) gives a compact formula for the expected number of inclusions in the slab

$$\langle N \rangle = \sum_{n=0}^{\lfloor L/\Delta x \rfloor - 1} \frac{\gamma\left(n+1, \lambda\left(L-(n+1)\Delta x\right)\right)}{(n)!}. \tag{38}$$

By inspection of Eq. (38) we see that the expected number of inclusions depends on both the total length of the slab, L, as well as the inclusion length Δx. For convenience when considering problems of different sizes it is advantageous to rewrite Eq. (38) in terms of the dimensionless scale parameter

$$m \equiv \frac{L}{\Delta x}, \tag{39}$$

which yields the final form

$$\langle N \rangle = \sum_{n=0}^{\lfloor m \rfloor - 1} \frac{\gamma\left(n+1, \lambda\,\Delta x\left(m-(n+1)\right)\right)}{(n)!}. \tag{40}$$

A simple Monte Carlo simulation was used to confirm the accuracy of Eq. (40). In the numerical experiment, multiple independent realizations of a 1-D binary stochastic material were created and used to estimate the ensemble average number of inclusions as a function of m and λ. For each realization, inclusions of width Δx were placed at random intervals within a slab of length $L = 1$. The spacing between adjacent inclusions was determined by sampling from an exponential distribution (Eq. (1)) with a given (fixed) value of λ. When no more inclusions will fit within the slab, the total number of inclusions for the realization is recorded and the process begins again for the next realization. After many realizations the population mean and variance can be used to estimate the expected (ensemble average) number of inclusions for the slab. Table I shows the results of 50,000 realization numerical experiments performed with different values of m and λ. In all cases the calculated ensemble average was found to agree to within statistical uncertainty with the expected value given by Eq. (40).

Unfortunately, for large values of m, determining $\langle N \rangle$ can be calculationally intensive. Furthermore, the form of Eq. (40) makes it difficult to solve accurately with a low order approximation, such as a truncated series expansion. However, in the next section we will show that it is possible to make a reasonable approximation for $\langle N \rangle$ based on physical arguments, and then bound the error of this approximation through numerical studies.

Table I. Comparison of analytical and statistical estimates for the expected number of inclusions in binary stochastic materials of length $L = 1$. Statistical estimates were generated with 50,000 independent realizations.

λ	m	$\langle N \rangle$	$\hat{N}$	$\sigma_{\hat{N}}$
1	10	0.8223	0.8209	4.052×10^{-3}
10	10	4.6250	4.6293	9.622×10^{-3}
100	1.01	0.6285	0.6267	3.540×10^{-3}
100	2.25	1.9998	1.9998	6.324×10^{-3}
100	5.5	4.9480	4.9482	9.948×10^{-3}
100	10	8.6664	8.6660	1.317×10^{-2}
100	100	49.625	49.642	3.150×10^{-2}

3. APPROXIMATING THE EXPONENTIAL RATE PARAMETER

3.1. Inclusion Volume Fraction

The derivations in Section 2 provided an analytical equation for the expected number of inclusions as a function of the geometric properties, L and $m = L/\Delta x$, and the rate parameter λ. The original objective, however, was to solve for the rate parameter as a function of the material properties. Unfortunately, Eq. (40) contains two unknown quantities, $\langle N \rangle$ and λ, so it will be necessary to find a second relationship between these quantities before a solution can be attempted. The required condition can be obtained from a volume balance equation, which relates the expected number of inclusions in the slab to the material properties L, Δx and V_B, defined as the total volume fraction occupied by material B in the slab. In this case, V_B is treated as a known material property, which may be obtained directly from manufacturing data (for man-made systems such as concrete, HTGR fuel elements, or BORAL®), or estimated through auxiliary measurements of the bulk material density and average inclusion size (for naturally occurring stochastic mixtures). In either case, for a fixed inclusion width of Δx, the expected number of inclusions is given by

$$\bar{N} = \frac{V_B L}{\Delta x} = V_B m \,, \tag{41}$$

where, again, V_B is the volume fraction of material B, as determined from physical measurements or manufacturing data.

Equation (41) provides the necessary relationship required to potentially solve for the unknown rate parameter, λ. Assuming that the distribution of distances between inclusions is well

represented by an exponential distribution, then the unknown rate parameter, λ, must satisfy the relationship $\langle N \rangle = \bar{N}$, where $\langle N \rangle$ is the expected number of inclusions (Eq. (40)) obtained by calculating the expectation value of $p(N)$ and $\bar{N}$ is the expected number of inclusions based on physical (mass/volume balance) conservation properties of the problem (Eq. (41)).

3.2. Single Inclusion Case

For cases where $\Delta x > L/2$ (i.e. $m < 2$) the expected value of $p(N)$ has a particularly simple form, as shown in Eq. (30),

$$\langle N \rangle = \gamma\left(1, \lambda\left(L - \Delta x\right)\right) = 1 - e^{-\lambda(L-\Delta x)} \qquad (\text{for } \Delta x > L/2). \tag{42}$$

Because of the simple form it is possible to analytically solve Eq. (42) for λ in terms of the expected number of inclusions $\langle N \rangle$,

$$\lambda = \frac{-\ln\left[1 - \langle N \rangle\right]}{\left(L - \Delta x\right)} \qquad (\text{for } \Delta x > L/2). \tag{43}$$

Applying the condition $\langle N \rangle = \bar{N}$, and using Eq. (41), yields the final result

$$\lambda = \frac{-\ln\left[1 - V_B m\right]}{\left(L - \Delta x\right)} \qquad (\text{for } \Delta x > L/2). \tag{44}$$

Again, we remind the reader that the expressions shown in Eqs. (43) and (44) are exact if the distribution of distances between inclusions (or in this case the distance between the inclusion and the edges of the slab) follow an exponential distribution. However, the denominator of Eq. (43) provides some indication about the limitations of this original assumption. As the inclusion width, Δx, approaches the total length of the slab, L, the denominator goes to zero, which causes the rate parameter to approach ∞. This result is in keeping with the physical realities of the problem, which dictate that as $\Delta x \rightarrow L$, the position of the inclusion within the slab becomes deterministic rather than stochastic. In this case, the use of an exponential distribution to describe the position of the inclusion within the slab is no longer appropriate. Instead, the Bernoulli distribution should be used to describe the probability that an inclusion will (or will not) be found in a particular observation of the stochastic material. This result is consistent with the results for the single inclusion case previously derived in section 2.5.

3.3. Multiple Inclusion Case

Unfortunately, inspection of Eq. (40) reveals that the equation cannot be easily inverted to solve for λ in terms of $\langle N \rangle$ for cases where $m \geq 2$. This eliminates the possibility of finding a simple, analytic, solution for λ that will cover all cases of interest. Instead, we will try to develop an approximate, easily invertible, relationship between $\langle N \rangle$ and λ that can be used to solve the

problem. In order to derive this approximate relationship we will use a low-accuracy approximation for the initial form of the rate parameter λ, and then attempt to apply correction terms in order to produce a more accurate final approximation for λ.

3.3.1. Approximation by a Poisson process

In order to find an initial approximation for λ, we return to the fact that our one-dimensional stochastic media problem is remarkably similar to a Poisson process, with distance traveled through space, rather than time, as the independent variable. In fact, the only difference between a slab containing randomly placed inclusions and a true Poisson process lies in the fact that the inclusions have a width, where a standard Poisson process assumes that the events occur instantaneously (in this case implying an inclusion width of zero). This observation was confirmed in section 2.5 where it was shown that the probability density function for the number of inclusions in the slab approaches a Poisson distribution in the limit as inclusion width approaches zero. Therefore, it is reasonable to expect that a one-dimensional stochastic material with small inclusions may be approximated by a homogeneous Poisson process, where

$$p\left(\left(N(x+\delta x)-N(x)\right)=n\right)=\frac{e^{-\tilde{\lambda}\delta x}\left(\tilde{\lambda}\delta x\right)^{n}}{n!} \tag{45}$$

is the probability that n inclusions will be observed between position x and $x+\delta x$ in the slab, and $\tilde{\lambda}$ is the probability per unit distance traveled that an inclusion will be observed. For a slab with total length L, the expected number of inclusions predicted by Eq. (45) is

$$\tilde{N}=\sum_{n=0}^{\infty} n\ p\left(N\left(L\right)=n\right)=\tilde{\lambda}L\,. \tag{46}$$

Setting the expected number of inclusions predicted by the Poisson model, $\tilde{N}$, equal to the expected number of inclusions predicted by mass and volume balance, $\bar{N}$, allows us to solve for $\tilde{\lambda}$ in terms of the physical dimensions of the model

$$\tilde{N}=\lambda_P L=\frac{V_{\mathrm{B}}L}{\Delta x}=\bar{N}$$

$$\lambda_P=\frac{V_{\mathrm{B}}}{\Delta x}\,. \tag{47}$$

While Eq. (47) may provide a reasonable approximation in cases when $\Delta x\to 0$ or $m = L/\Delta x\to\infty$, it is not sufficient for most problems of interest. As expected, the model breaks down for nonzero values of Δx because the inclusions are not instantaneous events.

3.3.2. Approximation by a modified Poisson process

To overcome this limitation, let us redefine the problem in terms of λ_A, which represents the probability per distance traveled in material *A* that an inclusion will be observed. The relationship between λ_A and λ_P is given by

$$\lambda_P L = \lambda_A L_A , \tag{48}$$

where L_A is the total length of material *A* in the problem. Unfortunately this relationship is complicated by the fact that L_A is a random variable that will depend on a particular realization of the problem. However, we can calculate the expected value of L_A from the physical mass and volume balance presented in Eq. (41). If the expected number of inclusions in the slab is given by $\bar{N}$ and the length of each inclusion is Δx it follows that

$$\langle L_B \rangle = \bar{N} \Delta x = V_B L , \tag{49}$$

and

$$\langle L_A \rangle = L - \langle L_B \rangle = (1 - V_B) L . \tag{50}$$

Substituting Eq. (50) into Eq. (48) gives

$$\tilde{\lambda} L \approx \lambda_A L (1 - V_B) . \tag{51}$$

Equation (51) can now be substituted into Eq. (46) to yield an approximation for $\tilde{N}$

$$\tilde{N} \approx \lambda_A L (1 - V_B) , \tag{52}$$

which, when set equal to $\bar{N}$, can be solved for λ_A,

$$\lambda_A = \frac{V_B}{(1 - V_B) \Delta x} . \tag{53}$$

For clarification, we note that λ_A is only an approximation and should not be viewed as an exact solution. However, we expect Eq. (53) to be a good approximation in cases where the amount of variability of L_A between realizations is small (implying V_B or $m = L/\Delta x$ is large). In fact, Eq. (53) is identical to the theoretical rate parameter for an infinite problem, as discussed in Reference 11.

3.3.3. Residual error due to modified Poisson approximation

Now that we have an approximation for the rate parameter, λ, we wish to determine how accurate this approximation is for problems of interest. To determine this accuracy, we will consider the

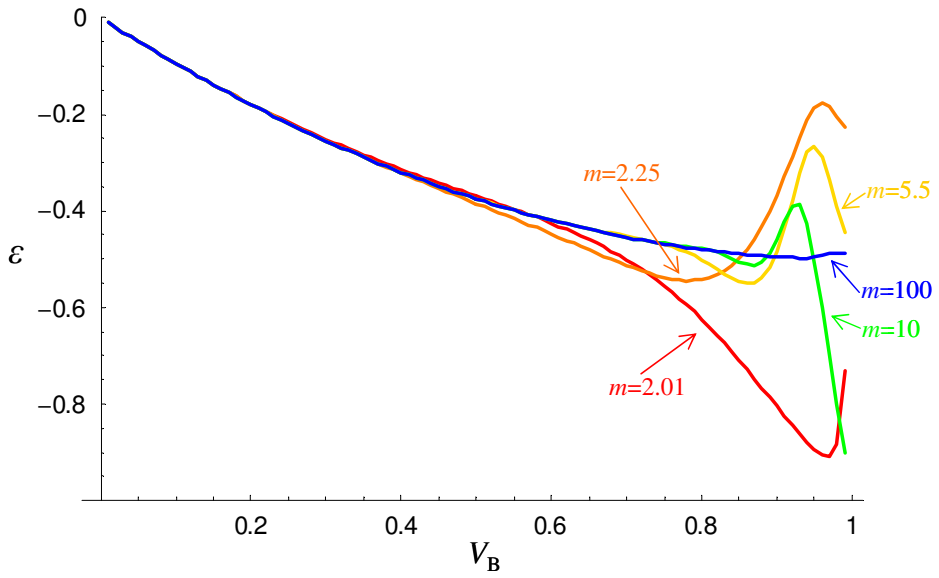

Figure 3. Error between the true expected number of inclusions and the expected number of inclusions predicted by the modified Poisson approximation, as a function of inclusion volume fraction V_B, for 5 values of m.

residual difference between the true mean $\langle N \rangle$ calculated by Eq. (40) using $\lambda=\lambda_A$, and the desired mean $\bar{N}$ as defined in Eq. (41),

$$\varepsilon = \langle N \rangle - \bar{N} = \left(\sum_{n=0}^{\lfloor m \rfloor - 1} \frac{\gamma\left(n+1,\, \lambda_A\, \Delta x\left(m-(n+1)\right)\right)}{(n)!} \right) - V_B\, m\,. \tag{54}$$

Unfortunately, due to the complexity of $\langle N \rangle$ no simple analytic form to describe the behavior of ε as a function of m and V_B has been found. Instead we have chosen to rely on numerical calculations to determine the behavior of ε over its domain.

Figure 3 shows a plot of ε versus V_B for 5 values of m, m=2.01, 2.25, 5.5, 10, and 100. Each plot was created from 100 equally spaced data points between $V_B = 0$ and $V_B = 1$. Figure 4 shows the same plot with 50 harmonically spaced values of m between 2 and 100 ($m=\{100/k\}_{k=1,50}$). All cases assume a fixed total slab length $L = 1$. From Figure 4 we see that ε appears to be bounded over its entire domain by $0 < \varepsilon <= V_B$. This implies using λ_A as an approximation for the true rate parameter λ will under predict the expected number of inclusions within a slab by less than V_B, with a maximum error of -1 occurring as the volume fraction of material B approaches 1.0. Furthermore, Figure 3 indicates that ε appears to converge to a second order polynomial in V_B as $m \to \infty$ Infinity. A least squares fit of the data for $m = 100$ shows that ε is well approximated by

$$\varepsilon \approx \frac{V_B^2}{2} - V_B\,, \tag{55}$$

especially for large values of m/V_B.

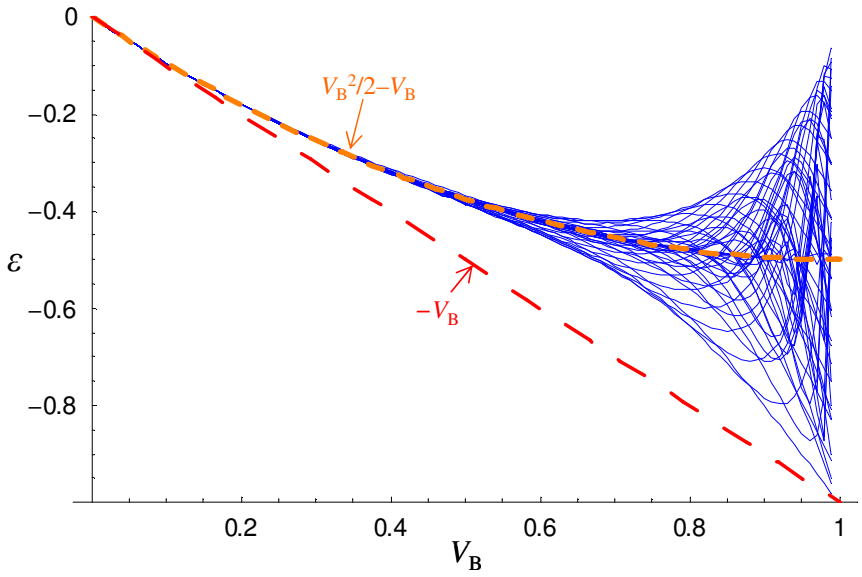

Figure 4. Error between the true expected number of inclusions and the expected number of inclusions predicted by the modified Poisson approximation, as a function of inclusion volume fraction V_B, for 50 harmonically spaced values of m between 2 and 100.

3.3.4. Approximation by a residual-error corrected Poisson process

By substituting the approximation for the residual error ε into Eq. (54) and rearranging, we can effectively "correct" the modified Poisson approximation in order to obtain a better approximation for $\langle N \rangle$

$$\langle N \rangle = \varepsilon + \bar{N} \approx \frac{V_B^2}{2} - V_B + V_B\, m\,,$$
$$\langle N \rangle \approx \tilde{N}_1 \equiv \frac{V_B^2}{2} + V_B\,(m-1)\,. \tag{56}$$

As before, we can numerically calculate the residual error between the true mean $\langle N \rangle$ calculated by Eq. (40) using $\lambda=\lambda_A$, and the approximation $\tilde{N}_1$ as defined in Eq. (56),

$$\varepsilon_1 = \langle N \rangle - \tilde{N}_1 = \left(\sum_{n=0}^{\lfloor m \rfloor - 1} \frac{\gamma\left(n+1,\, \lambda_A\, \Delta x\left(m-(n+1)\right)\right)}{(n)!} \right) - \left(\frac{V_B^2}{2} + V_B\,(m-1) \right). \tag{57}$$

Figure 5 shows a plot of ε_1 versus V_B for the same 5 values of m as shown in Figure 3. Again, each plot was created from 100 equally spaced data points between $V_B = 0$ and $V_B = 1$. Figure 6 shows the same plot with 50 harmonically spaced values of m between 2 and 100. Again, all cases assume a fixed total slab length $L = 1$. From Figure 6 we see that the residual ε_1 appears to be bounded over its entire domain by $|\varepsilon_1| < V_B^3/2$, a significant improvement over the residual bound of the uncorrected approximation, $|\varepsilon| < V_B$.

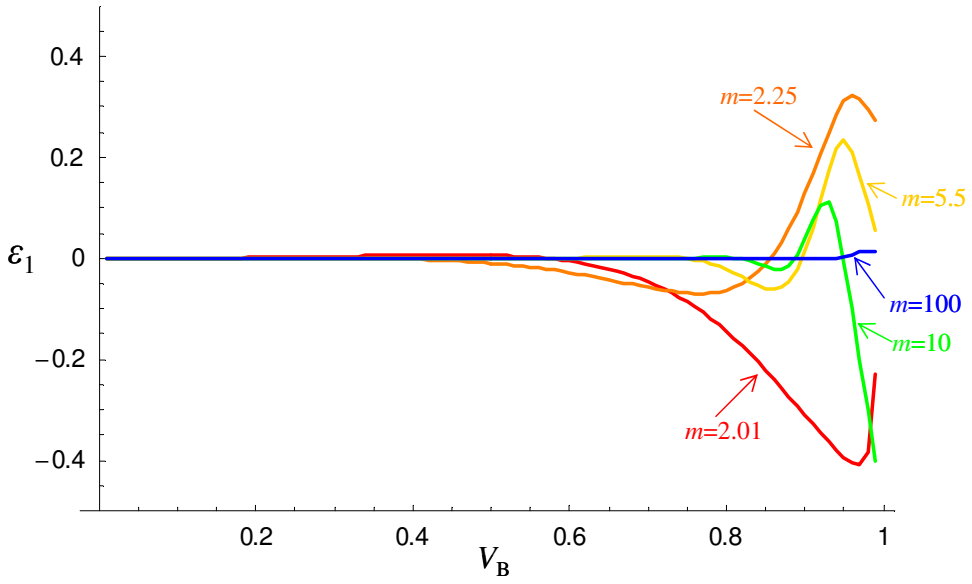

Figure 5. Error between the true expected number of inclusions and the expected number of inclusions predicted by the corrected Poisson approximation, as a function of inclusion volume fraction V_B, for 5 values of m.

At this point it is worthwhile to review the preceding approximations and discuss our current state relative to the original problem that was to be solved. Based on physical intuition we reasoned that, for a 1-D stochastic material with fixed inclusion widths, the spacing between inclusions can be approximated by a modified Poisson process where the rate parameter, λ_A, represents the probability of encountering an inclusion per distance traveled in the background material (material *A*). Through a series of numerical experiments it was confirmed that the expected number of inclusions predicted using the modified Poisson approximation does not agree with the expected number of inclusions calculated from the true probability density function for number of inclusions, given in Eq. (40). However, the residual difference between the expected number of inclusions calculated using the modified Poisson approximation and the true expected number of inclusions was found to be a simple, bounded function of the inclusion volume fraction and ratio of slab width to inclusion width for the problem. This result, shown in Eq. (57) implies that a system with rate parameter λ_A will produce an expected number of inclusions that is within $\pm V_B^3/2$ of $\tilde{N}_1$, or

$$\langle N \rangle = \sum_{n=0}^{\lfloor m \rfloor - 1} \frac{\gamma\left(n+1,\, \lambda\, \Delta x\left(m-(n+1)\right)\right)}{(n)!} \approx \frac{V_B^2}{2} + V_B\,(m-1)\,. \tag{58}$$

when

$$\lambda = \lambda_A \equiv \frac{V_B}{(1-V_B)\,\Delta x}\,. \tag{59}$$

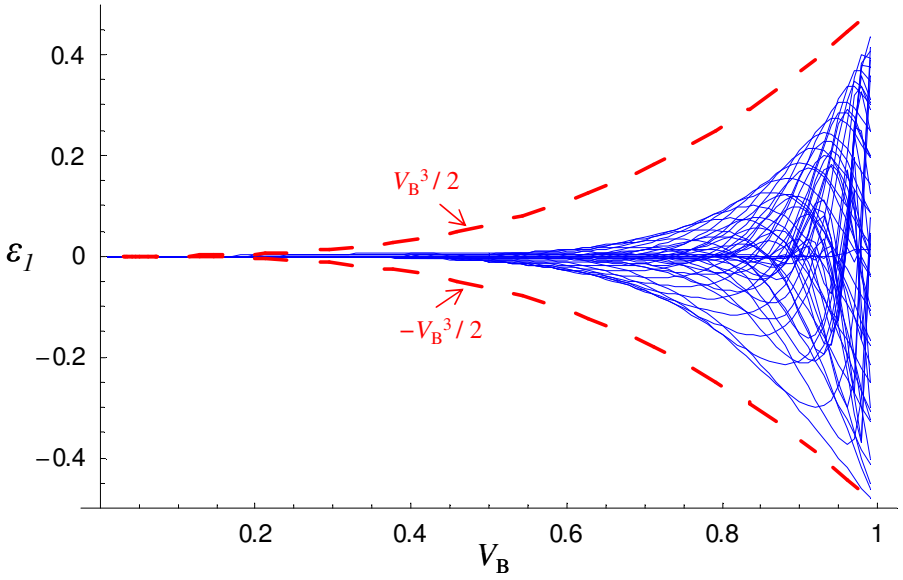

Figure 6. Error between the true expected number of inclusions and the expected number of inclusions predicted by the corrected Poisson approximation, as a function of inclusion volume fraction V_B, for 50 harmonically spaced values of m between 2 and 100.

3.3.5. Determining the effective rate parameter from the corrected Poisson approximation

Rearranging Eq. (58) gives a second order polynomial equation in V_B,

$$\frac{V_B^2}{2} + V_B(m-1) - \langle N \rangle \approx 0, \tag{60}$$

which can be solved to find V_B in terms of the expected number of inclusions, $\langle N \rangle$.

Before solving Eq. (60) for V_B we must first determine whether the polynomial will have a unique, real, positive root. To prove the existence of a solution we first rewrite Eq. (60) in the standard form for a quadratic equation,

$$aV_B^2 + bV_B + c = 0 \tag{61}a$$

where

$$a = \frac{1}{2}, \quad b = (m-1), \quad c = -\langle N \rangle \tag{61}b$$

To prove that the roots of Eq. (60) are real, we calculate the discriminant of the equation,

$$b^2 - 4ac = (m-1)^2 + 2\langle N \rangle. \tag{62}$$

Since $(m-1)^2$ and $\langle N \rangle$ are both positive values it follows that the discriminant is positive and Eq. (60) will always have real roots. To demonstrate the conditions under which Eq. (60) will have a unique positive root we factor the general form of the quadratic equation into a new form,

$$V_B^{\,2} + \frac{b}{a} V_B + \frac{c}{a} = \left(V_B - r_1\right)\left(V_B - r_2\right) = 0\,, \tag{63}$$

where r_1 and r_2 and the unknown roots of the equation. Expanding the right hand side of Eq. (63) yields,

$$V_B^{\,2} + \frac{b}{a} V_B + \frac{c}{a} = V_B^{\,2} - \left(r_1 + r_2\right) V_B + r_1 r_2 = 0\,. \tag{64}$$

Equating terms on the right and left hand sides of Eq. (64) gives a relationship between the coefficients of the equation its corresponding roots,

$$r_1 r_2 = \frac{c}{a} = -2\langle N \rangle\,. \tag{65}$$

Since, by Eq. (65), the product of r_1 and r_2 is less than zero, it follows directly that Eq. (60) must have one (and only one) positive root. Applying the quadratic equation to Eq. (60) gives an equation for the positive root,

$$V_B = 1 - m + \sqrt{\left(m-1\right)^2 + 2\langle N \rangle}\,. \tag{66}$$

Equation (66) provides a new relationship between the properties of the stochastic material (V_B and m) and the expected number of inclusions $\langle N \rangle$. The original relationship between these quantities, shown in Eq. (41), was developed from first principles by enforcing volume balance for inclusions within the slab. Unfortunately, while Eq. (41) provides an exact value for the expected number of inclusions within the slab, it cannot provide any information regarding the statistical distribution of distances between inclusions.

In order to obtain information on the distribution of distances between inclusions we assumed that the stochastic material could be well approximated by a Poisson (Eq. (47)) or modified Poisson (Eqs. (58) and (59)) process. This approximation provides the desired statistical prescription for the separation between inclusions, but leads to a different relationship between the expected number of inclusions in the slab $\langle N \rangle$ and the variables V_B and m, as shown in Eq (66). In cases where the two approaches predict the same number of inclusions for given values of V_B and m (i.e. Eq. (66) equals Eq. (41)) we may conclude that the modified Poisson approximation is valid and that the distance between inclusions is well approximated by an exponential distribution with rate parameter λ_A, given in Eq. (59).

Unfortunately, inspection of Eqs. (41) and (66) reveals that they cannot be expected to be equal for all values of V_B and m. In order to reconcile these potential differences, we recall that the

expected number of inclusions given by the volume balance approach, $\bar{N} = V_B m$ (Eq. (41)), is exact, while the modified Poisson process approach is only an approximation. Therefore, we wish to consider whether it is possible to "fit" the modified Poisson process in order to match the true expected number of inclusions, as determined by Eq. (41). This fitting can be accomplished by adjusting the inclusion volume fraction (and corresponding rate parameter) used in the modified Poisson process. From Eq. (66) we see that,

$$\tilde{V}_B = 1 - m + \sqrt{(m-1)^2 + 2\bar{N}} \,. \tag{67}$$

where $\tilde{V}_B$ is the effective inclusion volume fraction, which, when used in Eq. (58) gives an expected number of inclusions in the slab, $\langle N \rangle$, that is approximately equal to $\bar{N}$. Substituting Eq. (41) into Eq. (67) gives the relationship between the effective volume fraction and the true volume fraction,

$$\tilde{V}_B = 1 - m + \sqrt{(m-1)^2 + 2V_B m} \,. \tag{68}$$

Substituting the effective volume fraction into Eq. (59) gives the corresponding effective rate parameter, $\tilde{\lambda}$, for the material

$$\tilde{\lambda} = \frac{\tilde{V}_B}{\left(1 - \tilde{V}_B\right)\Delta x} \,. \tag{69}$$

3.3.6. Behavior of approximate rate parameter under limiting conditions

Notice that as $m \to \infty$, the effective volume fraction approaches the true volume fraction ($\tilde{V}_B \to V_B$) and the effective rate parameter approaches the modified Poisson rate parameter ($\tilde{\lambda} \to \lambda_A$). Noting that $L \to \infty$ as $m \to \infty$ (for fixed Δx), we see that Eqs. (68) and (69) correctly converge to the infinite medium results [11], again confirming that the modified Poisson process is exact as the inclusion width becomes small relative to the total slab length. For small values of m, the effective volume fraction and effective rate parameter will begin to diverge from the values predicted by the Poisson process. Therefore, the amount of deviation between $\tilde{V}_B$ and V_B (or $\tilde{\lambda}$ and λ_A) provides a direct measure of how well the distances between inclusions in the material may be approximated by a Poisson process.

Figure 7 shows the relationship between $\tilde{V}_B$ and V_B for several different values of m. For small values of m and V_B we see that there can be a significant difference (up to a factor of 2) between the true and effective volume fraction of the material. Inspection of Figure 7 also demonstrates that the effective volume fraction is always greater than the true volume fraction of the slab, a result that limits the range of applicability for using the modified Poisson process analysis with an effective volume fraction.

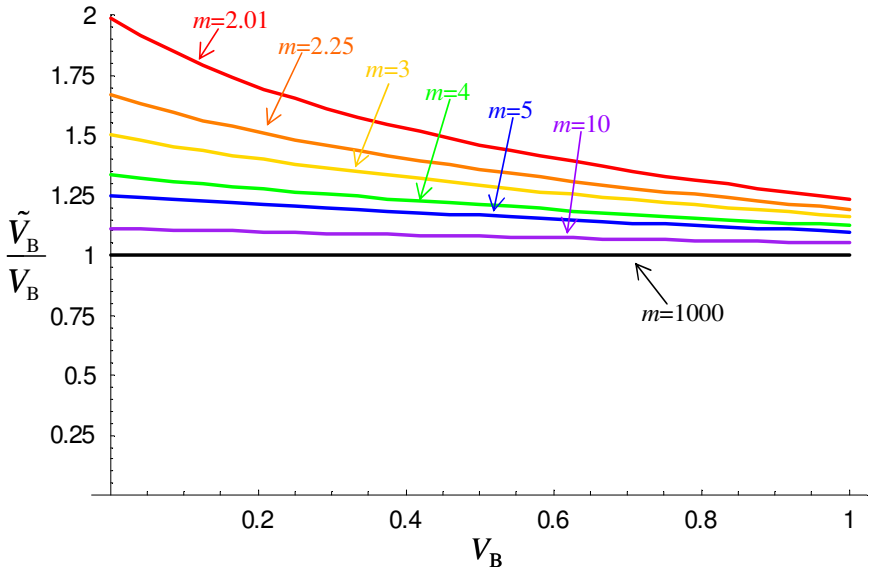

Figure 7. Relationship between effective and true inclusion volume fractions for 7 different values of *m*.

Due to the fact that inclusions are not permitted to extend beyond the end of the slab, there is a physical limit on the number of inclusions that will fit in a slab of given length. For a slab with length L and inclusion width Δx, the maximum number of inclusions allowed in the slab, without overlap, is equal to the integer part of $L/\Delta x$. From this observation, we can immediately see that the maximum possible inclusion volume fraction for a slab is given by,

$$\frac{\left\lfloor \frac{L}{\Delta x} \right\rfloor \Delta x}{L} = \frac{\lfloor m \rfloor}{m}. \tag{70}$$

This physical limit on the maximum volume fraction applies to both the true volume fraction of the material, V_B, as well as the effective volume fraction calculated from Eq. (68). Since it has already been established that $\tilde{V}_B > V_B$, we must consider $\tilde{V}_{B,max} = \lfloor m \rfloor / m$ to be the limiting case of interest. Setting the effective volume fraction (Eq. (68)) equal to the theoretical maximum volume fraction (Eq. (70)) and solving for V_B gives

$$V_{B,max} = \frac{\lfloor m \rfloor^2}{2m^3} + \frac{\lfloor m \rfloor (m-1)}{m^2}. \tag{71}$$

where $V_{B,max}$ is the maximum allowable true volume fraction. Materials with a true volume fraction larger than $V_{B,max}$ will have an effective volume fraction that does not satisfy Eq. (70). In these cases, the assumptions used to derive the empirical relationships used in the modified Poisson method begin to break down, producing unreliable results. Figure 8 shows a plot of the maximum true volume fraction, $V_{B,max}$, as a function of the dimensionless scale parameter m. This figure illustrates that $V_{B,max}$ has a saw tooth shape, with the values of the function bounded between the range $1–1/(2m)$ and $1–3/(2m)+1/(2m^3)$, depending on the fractional component of m.

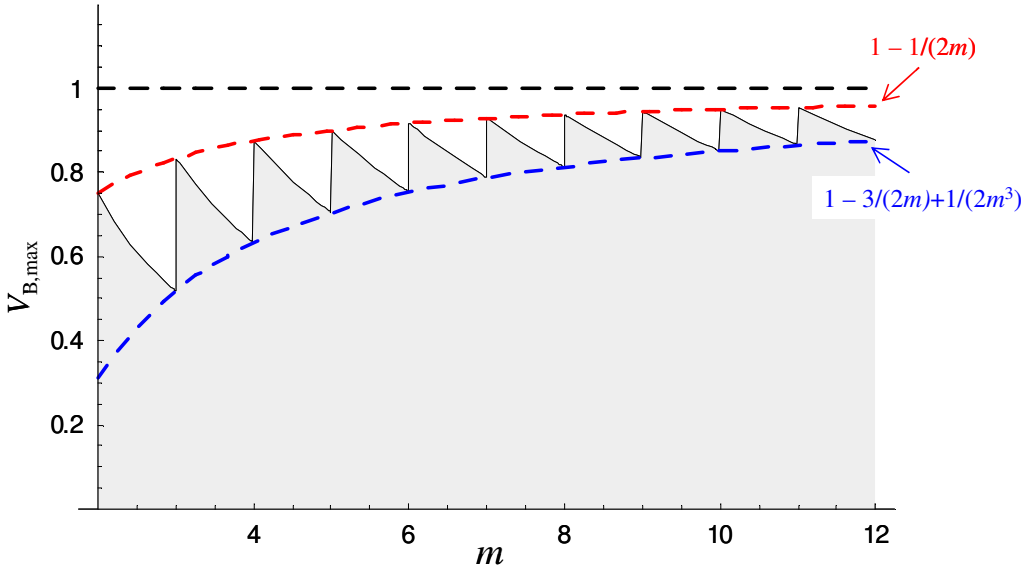

Figure 8. Plot of the maximum true volume fraction $V_{B,max}$ as a function of the dimensionless scale parameter m.

Based on these results, it is recommended that the modified Poisson approximation only be applied to materials with inclusion volume fractions below

$$V_{B,recommended} < 1 - \frac{3}{2m} + \frac{1}{2m^3}. \tag{72}$$

3.4. General Form of the Approximate Solution

Collecting the results from Eqs. (44), (68), and (69) gives the final results for the exponential rate parameter governing the distribution of distances between inclusions in a one-dimensional stochastic material,

$$\lambda = \begin{cases} \dfrac{-\ln\left[1 - V_B m\right]}{\left(L - \Delta x\right)} & 1 < m \le 2 \\ \dfrac{\tilde{V}_B}{\left(1 - \tilde{V}_B\right)\Delta x} & m > 2 \end{cases}, \tag{73}$$

where Δx is the width of the inclusions, L is the total length of the one-dimensional slab, m is the ratio of $L/\Delta x$, V_B is the true volume fraction of inclusions in the material, and $\tilde{V}_B$ is the effective inclusion volume fraction given by:

$$\tilde{V}_B = 1 - m + \sqrt{(m-1)^2 + 2V_B m}. \tag{68}$$

Table II. Comparison of analytical and statistical estimates for the expected number of inclusions in binary stochastic materials of length $L = 1$ and $m \leq 2$. Statistical estimates were generated with 50,000 independent realizations, where distances between inclusions were sampled from an exponential distribution with analytically derived rate parameter.

V_B	m	$\bar{N}$	$\hat{N}_\lambda$	$\sigma_{\hat{N}}$
0.8	1.001	0.8008	0.8024	4.006×10^{-3}
0.8	1.01	0.808	0.8052	4.013×10^{-3}
0.6	1.25	0.750	0.7518	3.878×10^{-3}
0.6	1.50	0.900	0.9006	4.244×10^{-3}
0.5	1.75	0.875	0.8748	4.183×10^{-3}
0.4	2.00	0.800	0.7986	3.997×10^{-3}

4. NUMERICAL RESULTS

The accuracy of the rate parameters shown in Eq. (73) was determined through a series of numerical experiments that were designed to cover a wide range of material properties (V_B and m). In each experiment, Eq. (73) was used to calculate the rate parameter for the material, λ, based on fixed values for V_B and m, and assuming L=1 in all cases. The same type of Monte Carlo simulation used to verify Eq. (38) was then used to estimate the expected (ensemble average) number of inclusions in the slab, $\hat{N}_\lambda$, for the calculated rate parameter. Individual numerical experiments used 50,000 independent realizations to produce the ensemble average, $\hat{N}_\lambda$. The calculated number of inclusions, $\hat{N}_\lambda$, can then be compared against the desired number of inclusions, $\bar{N}$, as calculated by Eq. (41). The relative accuracy of the rate parameter calculated from Eq. (73) can then be determined by measuring how closely $\hat{N}_\lambda$ approximates $\bar{N}$.

Table II shows the results for six stochastic mixtures, each with $m \leq 2$. For each of these stochastic materials the rate parameter λ was calculated from the exact single inclusion formula given in Eq. (44). As anticipated, the results in Table II demonstrate that the calculated ensemble average number of inclusions matches the predicted expected number of inclusions to within statistical uncertainty for all cases.

Table III shows the results for ten additional stochastic mixtures, this time with $m > 2$. For these stochastic materials the rate parameter λ was calculated from the approximation given in Eq. (69) and using the effective volume fraction given in Eq. (68). The results in Table III demonstrate that the calculated ensemble average number of inclusions agrees with the predicted number of inclusions to within 1% for most cases. However, the case with $m = 2.0001$ and $V_B = 0.5$ shows a difference of 6.5% between predicted and calculated results. For this particular case the volume fraction $V_B = 0.5$ is considerably larger than the recommended maximum volume fraction, $V_{B,recommended} = 0.3125$, calculated from Eq. (72). Table III also shows that the

Table III. Comparison of analytical and statistical estimates for the expected number of inclusions in binary stochastic materials of length $L = 1$ and $m > 2$. Statistical estimates were generated with 50,000 independent realizations, where distances between inclusions were sampled from an exponential distribution with approximate rate parameter.

V_B	m	$\bar{N}$	$\hat{N}_{\lambda_2}$	$\sigma_{\hat{N}}$
0.1	2.0001	0.2	0.2036	2.018×10^{-3}
0.2	2.0001	0.4	0.3983	2.822×10^{-3}
0.3	2.0001	0.6	0.6075	3.486×10^{-3}
0.4	2.0001	0.8	0.7941	3.986×10^{-3}
0.5	2.0001	1.0	0.9349	4.322×10^{-3}
0.5	3	1.5	1.5210	5.516×10^{-3}
0.5	4	2.0	1.9991	6.323×10^{-3}
0.8	10	8.0	7.9834	1.264×10^{-2}
0.9	10	9.0	8.9959	1.341×10^{-2}
0.95	20	19	18.999	1.949×10^{-2}

agreement between the calculated and predicted values appears to improve as the values of m increase, with agreement for the m=20 case reaching 0.005%.

A separate set of numerical experiments were conducted in order to quantify the relationship between the approximation error ($\varepsilon_1 = \bar{N} - N_\lambda$) and the physical properties of the stochastic material (m and V_B). Figure 9 shows a plot of the relative error between predicted and calculated number of inclusions, $\varepsilon_1 / \bar{N}$, versus m, the dimensionless ratio between the slab length (L=1) and inclusion width Δx. Each curve in Figure 9 shows the relative error for a particular inclusion volume fraction, V_B, which is itself a function of the scale parameter m for the material. The plot includes results for two volume fractions, the maximum allowable and recommended maximum volume fractions, $V_B = 1-1/(2m)$ and $V_B = 1-3/(2m)+1/(2m^3)$, respectively. For each case the approximation error was calculated from Eq. (57), using the effective rate parameter calculated from Eq. (69). Each curve was plotted with 5,000 equally spaced points between m=2 and m=10. Figure 9 illustrates the complex relationship between the relative error and the material parameters, V_B and m. As expected, the accuracy of the effective rate parameter decreases for small values of m, with the largest relative error for both cases occurring between m=2 and m=3. The large difference between the maximum relative error for both cases also demonstrates the breakdown of the effective rate parameter model as V_B approaches the maximum allowable value of $V_B = 1-1/(2m)$. Materials with volume fractions of $1-1/(2m)$ reach a maximum relative error of roughly 25%, while materials with volume fractions at the recommended maximum value of $V_B = 1-3/(2m)+1/(2m^3)$ exhibit a maximum relative error of less than 2.5%. Due to the complex interplay between the independent variables, especially the discontinuities that occur at integer

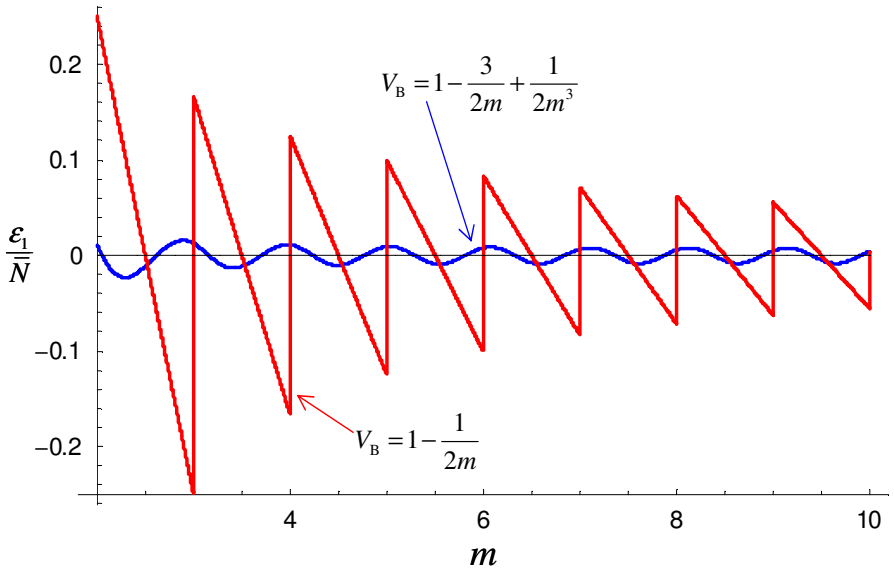

Figure 9. Plot of the relative error between predicted and calculated number of inclusions, $\varepsilon_1/\bar{N}$, versus as a function of the dimensionless scale parameter m.

values of m, readers should be aware that it is not possible to establish this 2.5% relative error as a rigorous upper bound for all materials with $V_B < V_{B,recommended}$. However, as we will demonstrate in the next study, this value is a reasonable approximation of the bound.

In order to further quantify the error of the approximation for $\langle N \rangle$, given in Eq. (58), as a function of the material properties V_B and m, and additional set of numerical experiments were conducted. These experiments were designed to determine the largest inclusion volume fraction that would result in the absolute value of the approximation error ε_1 (Eq. (57)) being less than or equal to a constant value, as a function of the scale parameter m. The resulting iso-error plots from these experiments are shown in Figure 10, for 6 different absolute errors. Each curve was generated by first calculating the absolute error of the approximation error (computed from Eq. (57)) at 200 equally spaced values of V_B between 0 and 1, for a fixed value of m. The 100 resulting values for ε_1 were then searched in ascending order by volume fraction to find the first value that exceeded the reference error for the curve. This process was then repeated for 490 equally spaced values of m, ranging from 2 to 100, in order to produce the curves shown in Figure 10.

The results shown in Figure 10 indicate a well defined relationship between the accuracy of the approximation and the material properties V_B and m. As expected, the accuracy tends to decrease as m becomes small and V_B becomes large. For values of m less than 10, the accuracy of the method begins to fall off sharply for inclusion volume fractions greater than roughly 50%. However, for larger values of m (m>25), the approximation shows excellent agreement with theoretical results, with errors on the order of 1×10^{-6} (absolute) for inclusion volume fractions up to 80%.

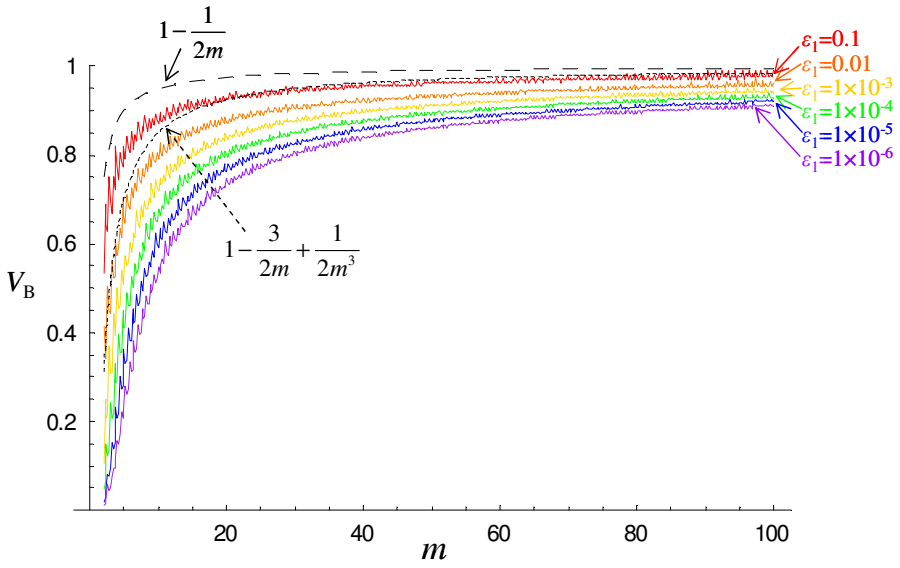

Figure 10. Iso-error plots showing the largest allowable inclusion volume fraction for a given level of absolute accuracy (ε_1), as a function of the dimensionless scale parameter m.

5. CONCLUSIONS

A new technique for characterizing the distribution of inclusions in a one-dimensional binary stochastic material has been developed. For materials where the distances between adjacent inclusions are exponentially distributed, an exact probability distribution for the number of inclusions in the slab has been derived. The resulting probability density function (pdf) has been shown to correctly reproduce known results in both the thin slab (Bernoulli distribution) and thick slab (infinite medium nearest neighbor distribution) limits. Unfortunately, due to the complex nature of the generalized pdf, the expected number of inclusions in a slab cannot be efficiently calculated. However, a simple, second-order polynomial approximation for the expected value of the pdf has been developed from empirical studies. It was subsequently shown that this simple approximation can be used to estimate the rate parameter of the exponential distribution based on the physical properties of the material. The resulting approximation is easy to implement, computationally efficient, and shows excellent agreement with theoretical results. Additionally, the new technique for approximating the rate parameter is shown to be equivalent to the infinite media nearest neighbor distribution with an effective inclusion volume fraction to account for the finite nature of the material. This result lends additional theoretical support to the volume adjustment factors that have been applied in techniques by Murata *et. al.* [7], Ji and Martin [11], and others.

Theoretical results provided in the paper are supported by numerical experiments, which have been conducted to determine the accuracy of the approximate rate parameter over a wide range of material properties. The results of these experiments demonstrate that the proposed rate parameter estimate provides an excellent approximation to the true rate parameter for many problems of interest. Further experiments confirm that the estimated rate parameter can be used to generate valid finite-length one-dimensional stochastic material realizations on the fly.

ACKNOWLEDGEMENTS

The authors would like to acknowledge Dr. Tom Sutton and Dr. Tim Donovan of the Knolls Atomic Power Laboratory and Prof. Ziya Akcasu of the University of Michigan for their helpful comments and suggestions regarding this work.

REFERENCES

1. G.C. Pomraning, "Transport Theory in Stochastic Mixtures," *Trans. Am. Nucl. Soc.*, 64, pp.286-287 (1991).
2. G.B. Zimmerman and M.L. Adams, "Algorithms for Monte Carlo Particle Transport in Binary Stochastic Mixtures," *Trans. Am. Nucl. Soc.*, 64, pp.287-288 (1991).
3. T.J. Donovan and Y. Danon, "HTGR Unit Fuel Pebble k-infinity Results Using Chord Length Sampling," *Trans. Am. Nucl. Soc.*, 89, pp.291-292 (2003).
4. T.J. Donovan and Y. Danon, "Application of Monte Carlo Chord-Length Sampling Algorithms to Transport through a Two-Dimensional Binary Stochastic Mixture," *Nucl. Sci. Eng.*, 143, pp.226-239 (2003).
5. D.R. Reinert, Investigation of Stochastic Radiation Transport Methods in Random Heterogeneous Mixtures, Ph.D. Dissertation, University of Texas, Austin (2008).
6. I. Murata, T. Mori, M. Nakagawa, "Continuous Energy Monte Carlo Calculations of Randomly Distributed Spherical Fuels in High-Temperature Gas-Cooled Reactors Based on a Statistical Geometry Model," *Nucl. Sci. Eng.*, 123, pp.96-109 (1996).
7. I. Murata, *et. al.*, "New Sampling Method in Continuous Energy Monte Carlo Calculation for Pebble Bed Reactors," *Journal of Nuclear Science and Technology*, 34, pp.734-744 (1997).
8. F. Brown, *et. al.*, "Stochastic Geometry and HTGR Modeling with MCNP5," *Proceedings of the Monte Carlo 2005 Topical Meeting, The Monte Carlo Method: Versatility Unbounded in a Dynamic Computing World*, CD-ROM (2005).
9. W. Ji and W.R. Martin, "Monte Carlo Simulation of VHTR Particle Fuel with Chord Length Sampling," *Proceedings of the Joint International Topical Meeting on Mathematics & Computation and Supercomputing in Nuclear Applications (M&C + SNA 2007)*, CD-ROM (2007).
10. W.B. Doub, "Particle Self-Shielding in Plates Loaded with Spherical Poison Particles," *Nucl. Sci. Eng.*, 10, pp.299-307 (1961).
11. W. Ji and W.R. Martin, "Application of Chord Length Sampling to VHTR Unit Cell Analysis," Proceedings of the International Conference on the Physics of Reactors (PHYSOR 2008), CD-ROM (2008).
12. G.L. Olson, J.E. Morel, and E.W. Larsen, "Chord Length Distributions in Binary Stochastic Media in Two and Three Dimensions," *Trans. Am. Nucl. Soc.*, 89, pp.307-309 (2003).
13. M. Abramowitz and I.A. Stegun, *Handbook of Mathematical Functions with Formulas, Graphs, and Mathematical Tables*, U.S. Government Printing Office, Washington D.C. (1964).